

AD622272

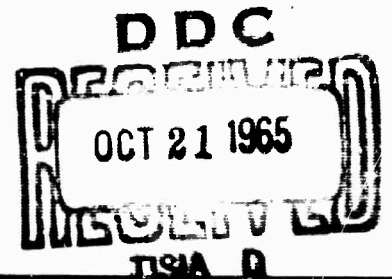
*Final Report*

**RESEARCH ON METASTABLE SPECIES  
IN ATOMIC MOLECULAR BEAMS  
PRODUCED BY CHARGE TRANSFER**

*Sponsored by:* ADVANCED RESEARCH PROJECT AGENCY  
PROJECT DEFENDER  
ARPA ORDER NO. 553

*Monitored by:* U.S. ARMY RESEARCH OFFICE - DURHAM  
UNDER CONTRACT DA-31-124-ARO-D-220

CLEARINGHOUSE FOR FEDERAL SCIENTIFIC AND TECHNICAL INFORMATION			
Hardcopy	Microfiche		
\$ 2.00	\$ 0.50	38	pp a2
ARCHIVE COPY			



STANFORD RESEARCH INSTITUTE

MENLO PARK, CALIFORNIA



**BEST  
AVAILABLE COPY**



September 20, 1965

*Final Report*

**RESEARCH ON METASTABLE SPECIES  
IN ATOMIC MOLECULAR BEAMS  
PRODUCED BY CHARGE TRANSFER**

*Sponsored by:* ADVANCED RESEARCH PROJECT AGENCY  
PROJECT DEFENDER  
ARPA ORDER NO. 553

*Monitored by:* U.S. ARMY RESEARCH OFFICE - DURHAM  
UNDER CONTRACT DA-31-124-ARO-D-220

*By:* D. C. LOFF                      R. PETERSON

*SRI Project PAU-5027*

*Copy No.* **158**

## SYNOPSIS

It is clear that excited atomic and molecular species play an important role in reentry phenomena. To understand and predict these phenomena, measured cross sections involving the excited species are required. A practical and general method of producing beams of metastable atoms and molecules is needed in order to measure these cross sections. For this use, near-resonant electron capture reactions are shown to produce excited neutral beams from ion beams with high efficiency.

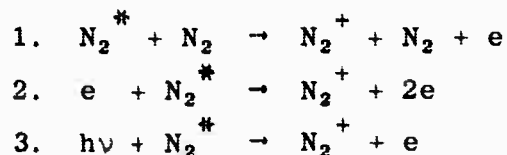
Total electron capture cross sections have been measured for the ions  $\text{He}^+$  and  $\text{Ar}^+$  in Rb and Cs in the energy range from 10 to 1500 eV. In these reactions, near energy resonances with the lowest metastable and allowed excited states of He and Ar occur, and capture into these states should be preferred. Cross sections ranging from 0.3 to  $1.7 \times 10^{-14} \text{cm}^2$  were measured, the magnitude of which indicates that most of the reactions lead to excited states. A preliminary experiment with  $\text{N}_2^+$  in Na gives strong indication of efficient production of excited  $\text{N}_2$ . Further studies are required to delineate the population of individual excited states. It is concluded that this technique of producing beams of metastable atoms and molecules is very promising and should be fully developed.

## CONTENTS

SYNOPSIS . . . . .	ii
OBJECTIVES AND ACHIEVEMENTS . . . . .	1
I INTRODUCTION . . . . .	3
II CHARGE TRANSFER CROSS SECTION MEASUREMENT . . . . .	6
A. The Apparatus . . . . .	6
1. Vacuum Chamber . . . . .	6
2. Ion Source and Beam Focusing . . . . .	7
3. Elements of the Interaction Chamber . . . . .	7
Vapor Beam Source . . . . .	7
Slow Ion Trap . . . . .	8
Vapor Beam Monitor . . . . .	9
B. Procedure . . . . .	11
C. Calculation of the Cross Sections . . . . .	13
III DISCUSSION OF THE RESULTS . . . . .	15
IV FUTURE WORK . . . . .	18
V CONCLUSION . . . . .	19
REFERENCES . . . . .	20
TABLE I Energy Defects for Initial Ground States and Various Neutral Atom Final States . . . . .	23
TABLE II Charge Transfer Cross Sections ( $10^{-14} \text{cm}^2$ ) for He and Ar Ions at Various Energies (eV) and Speeds ( $10^7 \text{cm/sec}$ ) in Rb and Cs Vapors . . . . .	24
Figure 1 Configuration of the Beam Interaction Region . . . . .	27
Figure 2 Retarding Potential Curve for $\text{Ar}^+$ . . . . .	28
Figure 3 Slow Ion Current Saturation Curves . . . . .	29
Figure 4 Vapor Beam Detector Responses vs. Oven Position . . . . .	30
Figure 5 Cross Sections for $\text{He}^+$ on Rb and Cs vs. Energy . . . . .	31
Figure 6 Cross Sections for $\text{Ar}^+$ on Rb and Cs vs. Energy . . . . .	31
Figure 7 Cross Sections for $\text{He}^+$ on Rb and Cs vs. Velocity . . . . .	32
Figure 8 Cross Sections for $\text{Ar}^+$ on Rb and Cs vs. Velocity . . . . .	32
Figure 9 Preliminary Cross Sections for $\text{N}_2^+$ on Na vs. Energy . . . . .	33

## OBJECTIVES AND ACHIEVEMENTS

Much attention has been given to reactions among ground state atmospheric species and between atmospheric species and contaminants such as sodium which occur in the shock fronts and wakes of reentering vehicles. At the same time little consideration has been given to the effects of excited particles which obviously exist in great numbers in these gases. We cite, for example, three classes of reactions which are important in reentry-excited gases:



Excited  $N_2$  is used as an example but these reactions will proceed with any long-lived excited species occurring in high temperature gases. Reactions of Class 1 have been shown to be an essential step in the initiation of ionization in shock waves.<sup>1</sup> The examples given above are all electron-producing, but many other reactions involving excited species (e.g., charge transfer, ion-molecule reactions, and de-excitation reactions) play significant roles in determining the electron production and recombination properties of the plasma.

One of the main reasons excited state reactions have been neglected in models of shocks and wakes is that very little is known about them. Rate constants and cross sections are judged to be large but have not been determined. This state of affairs is primarily due to the absence of experimental techniques capable of producing excited particles for direct study.

The research reported here was undertaken to develop such a source of metastable atoms or molecules which would permit direct studies of two-body interactions. Near-resonant electron capture reactions are being explored as a means to convert beams of ions to beams of excited neutrals. To demonstrate this technique, we have begun by studying electron capture by  $He^+$  and  $Ar^+$  from Rb and Cs. These reactions populate metastable levels of He and Ar; they were chosen because of the ease with

which they could be studied. However, the method can be applied equally well to many other species including the atmospheric. We have in fact shown that excited  $N_2$  must be produced in large amounts in the reaction



The effort thus far has clearly demonstrated a practical means of obtaining beams of neutral atoms or molecules containing a substantial portion (20 - 50%) of particles in long-lived excited states. Further work is needed to delineate the exact relative population of excited and ground states. The mature development of the technique will certainly lead to the study and understanding of excited state reactions such as those listed above.

## I INTRODUCTION

Symmetric-resonant electron capture reactions of the type



because of their large cross sections, are well known to be efficient in producing ground state neutral atoms from ions.<sup>2</sup> The nonsymmetric reactions



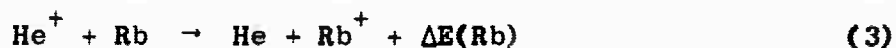
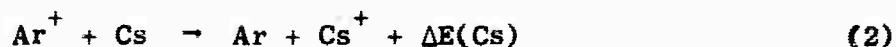
which involve an electronic transition, are generally characterized by comparatively small cross sections when the energy defect  $|\Delta E|$  is a few eV. On the other hand, several accidentally resonant ( $\Delta E \approx 0$ ) reactions between ground state particles have been studied<sup>3</sup> and were found to have large cross sections. Theoretically there should be no difference between a near-resonant reaction to an excited final state and one to a ground final state; hence large cross sections are expected for capture to excited final states when  $\Delta E$  is very small. Reactions of this type were observed and discussed, for instance, by Lindholm,<sup>4</sup> and by Dehmelt and Major,<sup>5</sup> but no cross sections were established. Indeed, electron capture reactions with near-resonant transitions to excited states should be very common among some reactants and their cross sections should usually be large. It is advantageous to put these circumstances to use: Near-resonant reactions may be selected to produce neutral beams populated in the excited states desired for specific experiments. Shortly after our work was begun, Donnally *et al.*<sup>6</sup> reported the measurement of the cross section for the reaction  $H^+ + Cs \rightarrow H(2s) + Cs^+$ . They found a large cross section of about  $4 \times 10^{-15} \text{ cm}^2$  ( $\Delta E$  is  $-0.49$  eV).

The most propitious conditions for populating a single specific excited state as a charge transfer product are:

- (1) The energy defect  $\Delta E$  (the potential energy converted to kinetic energy) for electron capture into the specified state is zero or very small
- (2)  $|\Delta E|$  is substantial (several eV) for all other possible final states
- (3) Low incident ion energies are used.

Thus the reaction must be asymmetric, as  $A^+ + B \rightarrow A^* + B^+$ , and near-resonant when the excited state is produced.

For atoms, these requirements are best met in certain rare gas ion-neutral alkali atom combinations. Here the reactions whose products are both in the ground state are highly nonresonant (large  $\Delta E$ ), and one can expect to populate metastable states of rare gas atoms in reactions which are very nearly resonant. We have selected combinations of  $Ar^+$  and  $He^+$  with Rb and Cs as the initial reactants. These afford the most clearly defined problems, and offer some experimental advantages for detection and diagnosis. The energy defects,  $\Delta E$ , for the reactions



are given in Table I for ground initial states (values for both the  $^2P_{3/2}$  and  $^2P_{1/2}$  states of  $Ar^+$  are included) and several final atom states, with the final ion in its ground state. Reactions (3) and (4) can also have close energy resonances when a ground state He atom and an excited ion are produced. Such reactions, of course, involve more than a single electron transition.

We have measured total capture cross sections for  $He^+$  and  $Ar^+$  beams in Rb and Cs over an energy range of 10 to 1500 eV for the above four reactions.<sup>7</sup> We have also made some cursory measurements on the reaction  $N_2^+ + Na \rightarrow N_2 + Na^+$  between 50 and 450 eV. For the noble gas-alkali reactions we find cross sections that increase nonuniformly with increasing energy; their magnitudes range approximately from 0.5 to  $1.5 \times 10^{-14} \text{cm}^2$ . For electron capture to the ground state, the reactions are highly non-resonant ( $\Delta E > 10 \text{ eV}$ ); thus the ground state cross sections are probably smaller than  $10^{-16} \text{cm}^2$ . The magnitude of our cross sections is therefore indicative of electron capture mainly to excited states.

In both He and Ar, short-lived states as well as metastable states will be populated, but at the present time no knowledge concerning the

relative populations of these states is available. Further research is therefore needed to determine the fraction of the neutral beam remaining in metastable states after the short-lived states have had time to decay. However, it has been confirmed that conversion of ion beams to excited neutrals by this method can be done efficiently. With a properly designed system it should be possible to convert 30 to 50% of the ions in a beam to excited neutrals, 20 to 50% of which will remain in metastable states. This efficiency may be contrasted with that of the electron bombardment method which has been used for many years to produce beams of excited particles at thermal velocities. The use of very intense electron beams to excite or ionize a large fraction of a neutral beam has been investigated by several people.<sup>8</sup> A practical upper limit to the fraction of a thermal beam which can be ionized is about 1%; and since excitation cross sections are generally smaller than ionization cross sections, the upper limit for the excitable fraction is probably less than 1%.

## II CHARGE TRANSFER CROSS SECTION MEASUREMENT

The experiment employs the crossed-beam arrangement shown in Fig. 1. An ion beam of variable energy passes perpendicularly through a thermal beam of alkali vapor. The slow ions produced in the intersection region are trapped in an electric potential trough and are collected on the inner of three concentric cylindrical grids placed coaxially with the ion beam. The ion beam is collected and measured after it exits from the slow ion trap. The vapor beam passes through the transparent grid structure and is condensed on a copper plate cooled to about  $-5^{\circ}\text{C}$ . Its flux density is monitored by a hot-wire ionizer placed just in front of the condensing plate.

The charge transfer current  $i_G$  is related to the ion beam current  $i_T$ : for  $i_G \ll i_T$

$$i_G = i_T Q \int \rho dx, \quad (5)$$

where  $Q$  is the reaction cross section and  $\rho$  the atom density at point  $x$  along the ion beam path; it is assumed that  $\rho$  is constant over any cross sectional slice of the ion beam but may vary with  $x$ . These conditions are satisfied in the experiment. The effective limits of integration correspond, of course, to the boundaries of the vapor beam. To determine  $Q$ , we measure  $i_G$ ,  $i_T$ , and the monitor current  $i_J'$  from which we determine  $\int \rho dx$  by a method described below.

### A. The Apparatus

#### 1. Vacuum Chamber

There are two vacuum sections, each pumped by a 6" oil diffusion pump trapped by a refrigerated baffle. One section contains the ion source and beam focusing electrodes; the other contains the alkali vapor oven and other apparatus associated with the beam interaction region. The two sections are connected by a cylindrical channel (1" long x 0.2" in diameter) which permits the ion beam to pass but impedes the gas flow from the ion source section (at  $10^{-4}$  Torr) to the measurement chamber (at about  $1.5 \times 10^{-6}$  Torr). The base pressure in the chamber is about  $3 \times 10^{-7}$  Torr.

## 2. Ion Source and Beam Focusing

The ion source is of the electron bombardment type<sup>9</sup> and produces very quiet beams of ions down to about 10 or 15 eV. Retarding potential curves were taken to obtain the energy spread; an example for argon ions at 20 eV "nominal" energy (based on the ion source potential) is presented in Fig. 2. The differentiated curve shows the beam to have a distribution peaked at 15.5 eV with a spread (full width at half maximum) of 1.5 eV. A similar curve for helium peaked at 16 eV and had a spread of 3.2 eV. The beam energy characteristics varied slightly with source conditions but were generally constant during a single run. The difference between the most probable ion energy (15.5 eV in Fig. 2) and the nominal energy was determined whenever measurements were carried out below 50 eV. The resulting correction to the beam energy was most important for the lower energies, but it was also applied at the higher accelerating voltages.

The ion beam is focused by a three-element lens in the source chamber. The beam is defined in direction and cross sectional area by the 0.2" diameter channel between the two vacuum chambers and by a second aperture, also 0.2" in diameter, located about 4" downstream, in front of the beam intersection region. The focusing voltages are usually adjusted to maximize the current to the ion beam collector, located beyond the charge transfer region. The ion beam currents ranged from about  $4 \times 10^{-9}$ A at 11 eV to  $3 \times 10^{-6}$ A at 1 keV.

## 3. Elements of the Interaction Chamber

The essential components in this chamber were all housed in an aluminum box, which was kept cold during the runs in order to trap stray alkali vapor. A thermally insulated 1" copper rod passed through the vacuum wall and connected a dry ice-acetone bath to the box, which was thus maintained at about -10°C with the oven hot. Other cold surfaces mentioned in the text were cooled by thermal contact with the box.

Vapor Beam Source. The oven is essentially a soft iron cylinder with a removable top, sealed with a 0.010" nickel wire gasket. The exit orifice is rectangular in cross section and filled with a crinkle foil thin-tube collimator to give a well directed vapor beam (see Fig. 1).

The oven was heated by a molybdenum heater in the orifice wall to maintain high orifice temperatures for optimum beam collimation. The oven was loaded in a dry argon atmosphere and the alkali metal was covered with dry benzene until the chamber had been evacuated by a roughing pump. No radiation shielding was required on the oven for Rb and Cs, but a single shield was installed for Na.

The oven was mounted on a movable platform which could be raised or lowered mechanically outside the chamber. For background measurements and during the oven warm-up periods, the oven was left in the down position and the beam was stopped by a cold copper plate located 1/2" in front of the orifice and about 1/4" from the outer grid of the ion trap. A rectangular aperture was located in this wall just at the ion beam level to define the vapor beam when the oven was in the up position, as shown in Fig. 1. This arrangement provided vapor beam definition, simplified background measurements, and prevented excessive deposition of the alkali metal on the elements of the ion trap.

Slow Ion Trap. Three concentric grids,  $G_1$ ,  $G_2$ , and  $G_3$  in Fig. 1, and two guard rings,  $G_0$ , at each end of  $G_1$  were designed (a) to provide trapping fields for the slow ions, which were collected on  $G_1$ , and (b) to shield  $G_1$  from stray, charged particle currents produced outside the beam intersection region. The incident ion beam is defined in cross section and angle by a 0.020" aperture before it enters the slow ion trap, and the geometry is such that the beam cannot hit  $G_1$ . This fact was checked experimentally by using an aperture 0.010" in diameter; no change in the cross section resulted.

The cylindrical grids are made from 0.0015" diameter tungsten wires stretched between thin nickel rings (1.0", 1.5", and 2.0" in diameter) at each end. The wires are held in tension by three stainless steel screws on each ring, mounted on a Micalox plate at each end of the trap. The ion beam passes through a 0.785" hole in each plate. The grid wires are spaced to provide high transparency (>98% per grid) for both the vapor beam and the photons generated in the beam interaction zone.

During the design of the grid structure, measurements were made of the electric potential distributions obtained for different grid wire spacings and for several voltages on each grid. These distributions were used, along with the current-voltage curves made during the preliminary runs and actual measurements, to determine the proper operating potentials. Figure 3 shows the slow ion current to  $G_1$ , taken at an ion energy of 250 eV, plotted as a function of the potential  $X$  of various elements while the potentials of the remaining elements remained fixed. For most ion beam energies, the following potentials were used:  $V_{G_0} = 6 - 10V$ ;  $V_{G_1} = -3V$ ;  $V_{G_2} = 22.5V$ ; and  $V_{G_3} = 12V$ . At ion energies below 50 eV,  $V_{G_0}$  was reduced to minimize defocusing of the ion beam; in all cases the voltages were arranged so that reasonable variations in them produced no change in the current to  $G_1$ .

Vapor Beam Monitor. A hot-wire surface ionization detector was used to monitor the alkali vapor flux density. The tungsten wire and ion collector plates (copper) were mounted immediately in front of the vapor beam condensing plate as indicated in Fig. 1. The plates formed a vee-shaped collector, with a narrow slot-aperture running the full length of the plates at the apex to pass a sample of the vapor in line with the ion beam axis and the oven orifice. The wire, placed midway between the plates, was held in tension by a spring to preserve its straightness. The wire and the plates were long enough to sample the entire width of the vapor beam in the direction of the ion beam, so that the monitor "looked at" a thin horizontal slab of the entire vapor target presented to the ion beam. The diameter of the tungsten wire was measured with an accurate micrometer. About twenty measurements taken over the length of the wire were used to determine the average diameter:  $2.40 \pm .05 \times 10^{-3}$  cm.

In operation, the wire was kept a few volts negative with respect to the condenser plate (ground), and the collector plates were about -45V. This arrangement assured complete collection of the ions by the plates.

The ion yield of the hot wire had the following characteristics when the wire current was varied to change its temperature: For low vapor beam densities, such as those which would produce monitor currents

of  $10^{-9}$ A, the yield rose sharply when the wire current reached about 20 mA for Rb (about 15 mA for Cs), reached a plateau at about 35 mA, and remained constant up to the maximum wire current employed, 120 mA. For higher densities (producing monitor currents of  $10^{-6}$ A), the yield continued to increase as the wire current was raised from 20 to about 60 mA, beyond which no change occurred. The increased temperature required for saturation doubtless reflected a decrease in the desorption time for the alkali ions on the wire surface, as well as the competition with the rate of arrival of atoms on the surface. During the cross section measurements, the wire current was generally about 90 mA. Under these conditions the monitor yield was independent of changes in either the collector plate voltage or wire current, and we assume that 100% ionization and collection efficiencies obtained, as is possible for Cs and Rb.<sup>10</sup>

The monitor current  $i'_J$  obeys the relationship

$$i'_J = ew'v_m \int \rho' dx$$

where  $e$  is the electronic charge,  $w'$  the diameter of the wire,  $v_m$  the mean thermal speed of the vapor atoms in the beam, and  $\rho'$  the vapor density at the wire. Now  $\int \rho' dx$  is related to  $\int \rho dx$  (at the ion beam axis) by a geometric factor due to the angular divergence of the vapor beam. A separate experiment was required to establish the factor  $K$  defined as

$$K = \int \rho dx / \int \rho' dx. \quad (6)$$

To accomplish this, another hot tungsten wire ionizer was stretched between the ends of the ion trap along the position of the ion beam axis, and the surface ionization current  $i_J$  was collected on  $G_1$ . A typical plot of the currents  $i_J$  and  $i'_J$  as a function of the vertical position of the oven is given in Fig. 4. Both currents are quite linear with oven position when the beam is partially cut off by the aperture, indicating a fairly uniform flux at the orifice, but there is a slight ( $\sim 2\%$ ) variation at the ion axis on the "flat" peak. The zero of the currents in Fig. 4 was taken as the background current with the oven in the OFF position well below the beam-defining aperture (at an indicator setting of about 7, to the left of the numbers on Fig. 4). A similar background

subtraction procedure was used during the cross section measurements. The ratio  $i_J/i'_J$  is also plotted in Fig. 4. It remains constant at 1.95 over the region when the oven is near the center of the defining aperture at a position indicator reading of 22.5. This value (1.95) of the ratio is uncorrected for the microammeter errors. The corrected ratio was close to 2.35 and increased less than 5% over a decade increase in vapor beam flux as the oven temperature was increased. This variation reflected a slow change in the vapor flow pattern with pressure. The ratio was also found to be the same for Rb and Cs for the same vapor pressure in the oven as determined from vapor pressure-temperature curves. The value of K used for each run was taken from the experimental value at the oven temperature for that run.

The ratio

$$i_J/i'_J = w \int \rho dx / w' \int \rho' dx = (w/w')K$$

and  $w' = w$  by measurement. The ratio was used to determine the atom target density  $\int \rho dx$  in Eq. (5) from the monitor current  $i'_J$ :

$$\int \rho dx = \frac{i_J}{ewv_m} = K \frac{i'_J}{ew'v'_m} \quad (7)$$

## B. Procedure

Relative measurements were first taken in the following manner, using either Rb or Cs in the oven. With the aluminum box cooled, the oven was heated to the desired temperature while in the OFF position. About an hour's time was required until all temperatures (measured by suitably placed thermocouples) and background currents reached equilibrium values.

At the beginning of each run, the monitor current was recorded as a function of oven position to ascertain the location of the center of the vapor beam ON peak for the ensuing measurements. For each value of the ion energy, the currents  $i_{G_1}$  (slow ions from charge transfer),  $i'_J$  (vapor beam monitor), and  $i_T$  (ion beam collector) were measured first with the oven in the OFF position, then two or three values were taken with the oven in the ON position, and then again with the oven at OFF. The differences  $\Delta i_{G_1}$  and  $\Delta i'_J$  were determined from vapor beam ON and OFF

readings, and the quantity  $\frac{\Delta i_{G_1}}{\Delta i'_j i_T}$  gave the relative cross section,  $i_T$

being the total ion current with the vapor beam OFF. The oven temperature was usually set so that about 2% of the ion beam underwent charge transfer at 250 eV; that is,  $\Delta i_{G_1} \approx 0.02 i_T$ , and  $i_T$  was reduced by 2% when the oven was raised. Under these conditions Eq. (5) is valid and the slow ion yield is linear with  $\Delta i'_j$  and  $Q$ . As the ion energy was changed, checks were made to test the validity of the current readings. Toward higher energies the potentials on the ion collector suppressor grids and on the ion trap guard rings  $G_0$  were rearranged to prevent positive ions emitted from the ion collector from reaching  $G_1$  and to suppress the more energetic secondary electrons. At ion energies below 100 eV, these potentials were reduced appropriately to prevent distortion of the beam ion trajectories. In all cases, the relative cross section was independent of reasonable variations in any of the electrode potentials about their operating values.

The slow ion yields were linear with the vapor density; the cross sections were unaffected by a six-fold increase in the monitor current. The cross sections were also independent of the ion beam current.

In addition to the charge transfer ions, there also existed a slow ion current to  $G_1$  caused by photoionization of the vapor beam. The photons emanated from the ion source and the resulting slow ion background was essentially constant during a given run. This background contributed increasingly toward lower ion beam energies, as both the ion beam current and the charge transfer cross sections decreased. At beam energies below 150 eV it was necessary to determine the contribution to  $i_{G_1}$  due only to charge transfer by taking measurements with the ion beam off and on, with the alkali oven both in the ON and OFF positions, and performing appropriate subtractions. The low energy limit of the measurements was reached when the charge transfer ion current was reduced to a magnitude comparable to the photoionization background and the uncertainties in this double subtraction procedure (due mainly to beam instabilities) became prohibitive in size.

Collisional ionization of the vapor atoms by ion impact reactions, of the type  $A^+ + B \rightarrow A^+ + B^+ + e$ , can also yield slow ions. It was not possible in our apparatus to shield grid  $G_2$  against electrons from other sources in order to measure the electrons produced by the ionization reactions; however, Perel et al.<sup>11</sup> have reported that the total electron current from  $Rb^+ + Rb$  collisions at 10 keV was less than 1.5% of the charge transfer current. At an equivalent ion speed ( $1.5 \times 10^7$  cm/sec) the  $He^+ + Rb$  ionization cross section is probably no larger than that of  $Rb^+ + Rb$ , thus it should be less than 2% of the electron capture cross section. Although the ionization cross section for Cs may be somewhat larger, it is unlikely that any of the measured cross sections are increased by more than 5% due to this background. This effect is included in the total error estimated below.

### C. Calculation of the Cross Sections

The cross sections were obtained from the equation

$$Q = \frac{ew'v_m}{K} \cdot \frac{\Delta i_{G_1}}{i_T \Delta i'_J} \quad (8)$$

which follows from Eqs. (5) and (7), with  $i_G$  and  $i'_J$  replaced by  $\Delta i_G$  and  $\Delta i'_J$ , the changes in these currents caused by raising the vapor oven to the ON position. Again, the quantity  $\frac{\Delta i_{G_1}}{i_T \Delta i'_J}$  is the relative cross section described above,  $e$  is the electron charge,  $w'$  is the diameter of the hot wire of the vapor beam monitor,  $K$  is the monitor constant defined by Eq. (6), and  $v_m$  is the mean speed of the vapor beam atoms. For a vapor beam,  $v_m = \frac{8kT}{\pi m}^{1/2}$  and can be expressed as  $v_m = 1.46 \times 10^4 (T/M)^{1/2}$  cm/sec, where  $T$  is the oven temperature ( $^{\circ}K$ ) and  $M$  is the mass of the vapor atom (amu).

The cross sections for  $He^+$  and  $Ar^+$  in the vapors of Rb and Cs were measured over the ion energy range from about 10 to 1500 eV. The data appear in Figs. 5 - 8 and have been tabulated in Table II. The  $He^+ + Cs$  reaction cross section was studied the most thoroughly, and some energy points are not included in Table II. A few errors are indicated for low energy points. These are estimates of the experimental standard error.

When errors are not quoted, the experimental error is about 2% for  $\text{He} + \text{Cs}^+$  below 900 eV and 3% above, and about 3% for the other cross sections above 100 eV. In general, the error was less than 6% at the lowest energies. The total error is estimated to be less than 10%.

Preliminary measurements were also made for the reaction  $\text{N}_2^+ + \text{Na} \rightarrow \text{N}_2 + \text{Na}^+$ . The results are shown in Fig. 9. We were not able to establish the efficiency of the vapor beam monitor for Na. As expected,<sup>4</sup> the yield was quite dependent on the wire current, and so we simply ascertained that the vapor flux was constant and measured  $\frac{\Delta i_{G_1}}{i_T}$ . The effective value of the vapor flux was estimated from the measured oven temperature and corresponding Na vapor pressure, using the experimental  $\Delta i_{G_1}$  vs vapor-pressure relationship, which was found to be independent of mass for Rb and Cs. The accuracy of the absolute points is probably not worse than  $\pm 50\%$ . We experienced some difficulty with background in the measurements, and an indication of the relative accuracy is seen from the variation in three points (triangles) near the same energy, two of which were taken at the beginning and end of the same run; the third was from a different run. These data were taken in a very cursory manner and thus are only provisional; much more work needs to be done to bring them to the reliability of the other data. We did, however, feel that they were sufficiently significant to include in this report.

### III DISCUSSION OF THE RESULTS

The energy dependence of the cross sections obtained for total electron capture by  $\text{He}^+$  ions in Rb and Cs is shown in Fig. 5 and by  $\text{Ar}^+$  in Rb and Cs in Fig. 6. Velocity plots of these data are shown in Figs. 7 and 8. Three noteworthy features of these curves which will be discussed are the magnitude of the cross section, the general shape of the cross section curves, and the structure evident--particularly in the  $\text{He}^+ + \text{Cs}$  case.

The magnitude of these cross sections are larger than  $0.5 \times 10^{-14} \text{cm}^2$  except at the lowest energies. Cross sections of this magnitude can only result from a long-range interaction, i.e., at internuclear distances of the order of  $7 - 10 \times 10^{-8} \text{cm}$ . The fact that the interaction is effective at such large distances means that capture to excited states is predominant, since the ground state of a noble gas atom will not participate in such a long-range interaction because of its tightly bound closed-shell nature. This conclusion is consistent with qualitative predictions of near resonant charge transfer theory.<sup>12</sup> To derive reliable quantitative results from theory, wave functions for various states of the molecular ions formed in these collisions must be known as a function of internuclear separation. Reliable approximate functions are presently unavailable for the systems under study. Rapp and Francis<sup>13</sup> have applied the theory using very approximate wave functions derived from linear combinations of atomic orbitals. The very approximate nature of the theory and the fact that only a two-state case is considered make the application of their results to this problem of questionable value for quantitative comparison. However the qualitative behavior, which is consistent with that expected by Bates and Lynn and by Demkov, is probably correct.

The decrease in the cross sections as the velocity is decreased is consistent with the theoretical argument given by Bates and Lynn. They argue that in the case of nonsymmetric interactions an electronic transition such as electron capture cannot readily occur at low velocities where the molecular ion forms under near-adiabatic conditions. As the

velocity increases, transitions are induced by the perturbation resulting from the motion of the particles and the cross section increases to a maximum consistent with the Massey near-adiabatic relation. This qualitative behavior is observed most clearly in the  $\text{Ar}^+ + \text{Rb}$ ,  $\text{Ar}^+ + \text{Cs}$  collisions, where the levels of Ar which most likely participate all lie very close to one another in energy. In the He case the participating levels are more widely spaced which may account for the more gradual rise of the cross section as a function of ion speed. The fact that the cross sections do not decrease at high speeds may be due to the participation of additional electronic states.

The  $\text{He}^+ + \text{Cs}$  reaction has been studied with greatest care and the cross section clearly exhibits structure. There is evidence of structure in the other curves as well, but it is less well established. The structure on the velocity plot takes the form of slight bumps separated by rather definite breaks. Two possible explanations of the structure may be advanced. Because of the wide spacing of the excited levels of He, the structure may be simply manifesting the cross sections of individual excited states coming into prominence as the velocity increases. The Rapp-Francis calculation suggests this type of behavior, and Edmonds and Hasted<sup>3</sup> have explained the more prominent structure observed in the near resonant  $\text{I}^+ + \text{Hg}$  reaction on this basis.

On the other hand, the cross sections for the nonsymmetric reactions  $\text{Rb}^+ + \text{Cs}$  and  $\text{Cs}^+ + \text{Rb}$ , as well as the symmetric reaction  $\text{Rb}^+ + \text{Rb}$  obtained by Perel, Vernon, and Daley,<sup>11</sup> shown in Figs. 7 and 8, exhibit a small amplitude oscillatory structure similar in some respects to that observed in  $\text{He}^+ + \text{Cs}$ . Perel, Vernon, and Daley interpreted their subsidiary peaks by assuming that the target atom is initially excited by the incoming ion and that subsequently electron exchange between excited states occurs. Using the Rapp and Francis<sup>13</sup> approximations, they were able to find transitions corresponding to each of the peaks observed in the  $\text{Cs}^+ + \text{Rb}$  and  $\text{Rb}^+ + \text{Cs}$  combinations. However, this theory cannot explain the oscillations in the symmetric cases  $\text{Cs}^+ + \text{Cs}$  and  $\text{Rb}^+ + \text{Rb}$ , and it does not account for all the peaks in the  $\text{K}^+ + \text{Rb}$  data.<sup>14</sup> An alternative explanation has been given by Lichten<sup>15</sup> who suggests that

the oscillations in the total cross sections are manifestations of the oscillatory nature of the charge transfer probability observed in the differential cross section for both symmetric and nonsymmetric reactions.

Further experiments are necessary to determine the cause of this structure. A study of the excited states participating in the noble gas ion-alkali reactions will certainly provide a test of the first interpretation. A study of the differential scattering for these species should determine the role of Lichten's hypothesis.

A further complication which may contribute to the structure in the He reactions is the possibility of electron capture into the ground state with an associated excitation of the alkali ion. Such reactions can be nearly resonant in the case of He but are at least 1 eV nonresonant in the Ar - Cs case and 4 eV in the Ar - Rb case. The question of whether these ion-exciting capture reactions are somewhat suppressed, because they require two electronic transitions, cannot be answered until the state population of the beam is analyzed.

Measurements of the  $N_2^+ + Na$  cross section have not been completed. However, even these preliminary data in Fig. 9 are interesting because of the desire to produce excited  $N_2$  beams for investigations bearing on reentry shock and wake phenomena, and also because of the possible importance of the reaction itself in the lower ionosphere. The cross section is large and increases as the energy decreases (as in  $N^+ + O \rightleftharpoons O^+ + N$ ), indicative of a very close resonance in which case the  $N_2^*$  is excited by at least 10.5 eV. It is important to extend these measurements to lower energies to determine whether the cross section maximizes.

#### IV FUTURE WORK

Although many reactions of the type examined in this study need to be investigated, the major problem which remains to be solved is the determination of the capture cross section for each electronic state which is significantly populated. Two measurements which will provide the needed information were discussed in the semiannual report. One of these is a study of the capture into allowed states by a measurement of the radiation from the charge transfer zone. An accounting of all of the radiative state capture, together with total capture cross section, allows the metastable content of the beam to be determined--assuming no direct ground state capture. An optical pumping method in which metastable atoms in the beam are excited by photon absorption to higher states, whose subsequent reradiation is examined, permits the relative population of each of the metastable levels to be determined. Recently it has been claimed<sup>16</sup> that the ejection of electrons from a metal surface can be used to determine the metastable content of a He atom beam formed by charge exchange. In order to use this method, however, it was apparently assumed that secondary emission due to the ground state neutrals is negligible. This assumption needs to be carefully examined experimentally before the value of the technique can be assessed.

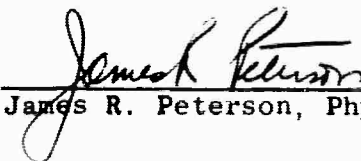
## V CONCLUSION

We have demonstrated that electron capture occurs readily in ion-atom collisions when a near energy resonance exists between the ground state of the initial atom and an excited state of the final atom or molecule. Although only a few reactions of this type have been studied, they will be generally characterized as having high cross sections. For this reason, reactions such as  $N_2^+ + Na \rightarrow N_2^* + Na^+$ , for example, may be of importance in reentry plasmas as well as in the lower ionosphere.<sup>17</sup> Further measurements on this reaction, beyond our preliminary work, are anticipated.

Furthermore, the high cross sections portend the use of these reactions to produce beams of excited atoms and molecules. In particular, it appears possible to produce beams of metastable atoms or molecules of sufficient density to be useful for a variety of crossed beam experiments. Certainly collisions between excited and ground state atoms resulting in ionization, excitation, or scattering can be studied. The major problem associated with the use of these beams in collision experiments is the determination of the state population of the beams. Solutions to this problem are being studied.



Donald C. Lorents, Chairman  
Department of Molecular Physics



James R. Peterson, Physicist

Approved: 

R. B. Vaile, Jr.  
Associate Executive Director, for  
Charles J. Cook, Executive Director  
Chemical, Theoretical, and Applied  
Physics Division

### ACKNOWLEDGEMENT

The authors are indebted to Mr. Ralph Leon for his able assistance in constructing and maintaining the equipment, and in preparing the apparatus for the experimental runs.

#### REFERENCES

1. H. S. Johnston and W. Kornegay, *Trans. Faraday Soc.* 57, 1563 (1961); *J. Chem. Phys.* 38, 2242 (1963); K. E. Harwell and R. G. John, *Phys. Fluids* 7, 214 (1964)
2. I. Amdur and A. L. Harkness, *J. Chem. Phys.* 22, 664 (1965); N. G. Utterback and G. H. Miller, *Rev. Sci. Instr.* 32, 1101 (1961); J. R. Peterson, in *Atomic Collision Processes*, M. R. C. McDowell, ed., North Holland Publ. Co. (1964) p 465
3. W. L. Fite, A. C. H. Smith, R. F. Stebbings, *Proc. Roy. Soc. (London)* A268, 527 (1962); R. F. Stebbings, A. C. H. Smith, and H. Ehrhardt, in *Atomic Collision Processes*, M. R. C. McDowell, ed. North Holland Publ. Co. (1964) p. 814; P. H. Edmonds and J. B. Hasted, *Proc. Phys. Soc.* 84, 99 (1964)
4. E. Lindholm, "Recombination Energies of Positive Atomic and Molecular Ions," Abstracts of Papers of the 2nd International Conference on the Physics of Electronic and Atomic Collisions, Boulder, Colorado, 1961, W. A. Benjamin, Inc., New York, p. 177
5. H. G. Dehmelt and F. G. Major, *Phys. Rev. Letters* 8, 213 (1962)
6. B. L. Donnally, T. Clapp, W. Sawyer, and M. Schultz, *Phys. Rev. Letters* 12, 502 (1964)
7. D. C. Lorents and J. R. Peterson, IV Int. Conf. Phys. of Electronic and Atomic Collisions, Quebec, 1965
8. R. Weiss, *Rev. Sci. Instr.* 32, 397 (1961); W. Aberth, *Rev. Sci. Instr.* 34, 928 (1963); A. G. Bennewitz and R. Wedemeyer, *Zeit. f. Physik.* 172, 1 (1963)
9. D. C. Lorents and W. Aberth, *Phys. Rev.* 139, A1017 (1965)
10. S. Datz and E. H. Taylor, *J. Chem. Phys.* 25, 389 (1956)
11. J. Perel, R. H. Vernon, and H. L. Daley, *Phys. Rev.* 138, A937 (1965)
12. D. R. Bates and N. Lynn, *Proc. Roy. Soc.* A253, 141 (1959); Y. N. Demkov, *Soviet Physics JETP* 18, 138 (1964)
13. D. Rapp and W. E. Francis, *J. Chem. Phys.* 37, 2631 (1962)
14. J. Perel, R. Y. Vernon, and H. L. Daley, IV Int. Conf. Phys. of Electronic and Atomic Collisions. Quebec, 1965
15. W. Lichten, *Phys. Rev.* 139, A27 (1965)

16. P. Mahadevan, C. E. Carlston, and C. D. Magnuson, *Bull. Am. Phys. Soc.* II 10, 692 (1965)
17. Neutral and ionized sodium are important constituents of the D-region of the ionosphere. See W. R. Bullock and D. M. Hunten, *Can. J. Phys.* 39, 976 (1961); R. S. Narcisi and A. D. Bailey, *Mass Spectrometry in the D-region Ionosphere--Apparatus, Techniques, and First Measurements*, AFCRL-65-81 (1965)

TABLE I  
 Energy Defects for Initial Ground States and Various Neutral Atom Final  
 States  
 (Final ion in ground state)

He <sup>+</sup> (1s)	ΔE(Rb)		ΔE(Cs)	
<b>He Final State</b>				
1S <sub>0</sub>	19.31		19.60	
2 <sup>3</sup> S	0.60		0.89	
2 <sup>1</sup> S	-0.21		0.08	
2 <sup>3</sup> P λ 10830	-0.56		-0.27	
2 <sup>1</sup> P λ 584	-0.81		-0.52	
Ar <sup>+</sup> Ion State	ΔE(Rb)		ΔE(Cs)	
	<sup>2</sup> P <sup>3</sup> / <sub>2</sub>	<sup>2</sup> P <sup>1</sup> / <sub>2</sub>	<sup>2</sup> P <sup>3</sup> / <sub>2</sub>	<sup>2</sup> P <sup>1</sup> / <sub>2</sub>
<b>Ar Final State</b>				
1S <sub>0</sub>	10.58	10.76	11.87	12.05
4s[ <sup>3</sup> / <sub>2</sub> ] <sub>0</sub> <sup>0</sup>	0.03	0.21	0.32	0.40
4s[ <sup>3</sup> / <sub>2</sub> ] <sub>1</sub> <sup>0</sup> λ 1067	-0.04	0.14	0.25	0.43
4s <sup>1</sup> [ <sup>1</sup> / <sub>2</sub> ] <sub>0</sub> <sup>0</sup>	-0.14	0.04	0.15	0.33
4s <sup>1</sup> [ <sup>1</sup> / <sub>2</sub> ] <sub>1</sub> λ 1048	-0.25	-0.07	0.04	0.22

TABLE II

Charge Transfer Cross Sections ( $10^{-14} \text{cm}^2$ ) for He and Ar Ions at Various Energies (eV) and Speeds ( $10^7 \text{cm/sec}$ ) in Rb and Cs Vapors

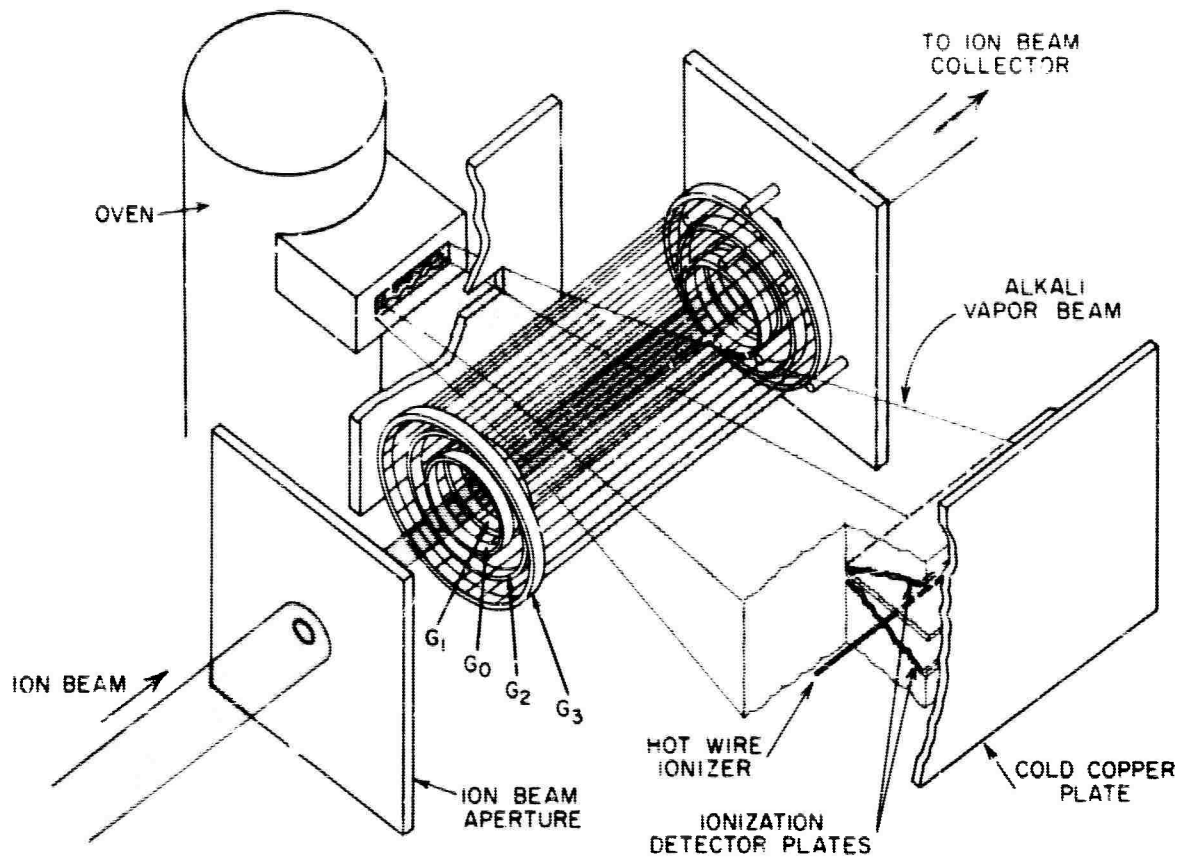
Energy	He <sup>+</sup>			Ar <sup>+</sup>		
	Speed	Q(Rb)	Q(Cs)	Speed	Q(Rb)	Q(Cs)
11	0.230		0.67±.06	0.073	0.46±.02	
16	0.278		0.66±.03	0.088	0.505±.02	0.320
21	0.318		0.63±.03	0.101	0.545±.01	
26	0.355		0.69±.01	0.112	0.595±.01	0.400
31	0.388		0.715±.01	0.122	0.665±.007	
36	0.417	0.36 1%	0.723±1%	0.132	0.700	0.445
41	0.445		0.720			
46	0.471	0.39	0.750	0.149	0.820	0.463
50	0.491		0.760			
56	0.520		0.785			
60	0.539		0.810			
65	0.560		0.825			
71	0.585	0.47	0.840	0.185	1.100	0.510
75	0.602		0.845			
80	0.622		0.853			
85	0.640		0.860			
90	0.660		0.870			
96	0.681	0.55	0.876	0.215	1.385	0.540
100	0.695		0.872			
105	0.712		0.870			
110	0.729		0.860			
115	0.745		0.858			
121	0.765	0.645	0.860	0.242	1.425	
125	0.777		0.875			
130	0.793		0.893			
140	0.822		0.923			
146	0.840			0.266	1.540	0.552
150	0.851	0.690	0.950			

TABLE II (continued)

Energy	He <sup>+</sup>			Ar <sup>+</sup>		
	Speed	Q(Rb)	Q(Cs)	Speed	Q(Rb)	Q(Cs)
160	0.880		0.975			
170	0.906	0.700	0.998	0.287	1.570	0.582
180	0.932		1.010			
190	0.958		1.020			
200	0.983	0.725	1.043	0.311	1.600	0.610
210	1.007		1.035			
225	1.030	0.720	1.045	0.330	1.590	
230	1.053		1.050			
240	1.075		1.070			
250	1.100	0.760	1.100	0.348	1.600	
275	1.150		1.170	0.365	1.630	
300	1.200	0.800	1.200	0.381	1.630	0.630
325	1.250		1.220	0.396	1.650	
350	1.300	0.832	1.250	0.411	1.650	
375	1.350		1.285	0.426	1.650	
400	1.390	0.865	1.325	0.440	1.655	
450	1.470	0.875	1.380	0.466	1.650	0.645
500	1.550	0.915	1.415	0.492	1.635	
550	1.630	0.990	1.445	0.516	1.650	0.655
600	1.700	1.005	1.470	0.539	1.655	
650	1.770	1.040	1.470	0.561	1.640	0.640
700	1.840	1.100		0.582	1.620	
750	1.900	1.130	1.530	0.602	1.630	0.730
800	1.960	1.150		0.622	1.630	
850	2.020		1.570	0.641	1.640	
900	2.080	1.250				
950	2.140		1.570	0.678	1.640	0.760
1000	2.200	1.265	1.580			
1050	2.250		1.590	0.713	1.640	
1150	2.360	1.350	1.640	0.745		0.680

TABLE II (continued)

Energy	He <sup>+</sup>			Ar <sup>+</sup>		
	Speed	Q(Rb)	Q(Cs)	Speed	Q(Rb)	Q(Cs)
1250	2.460	1.400		0.778	1.610	
1350	2.550		1.680	0.808		0.710
1450				0.837	1.630	
1495	2.680	1.445	1.655			



TB-5027-1

FIG. 1 CONFIGURATION OF THE BEAM INTERACTION REGION

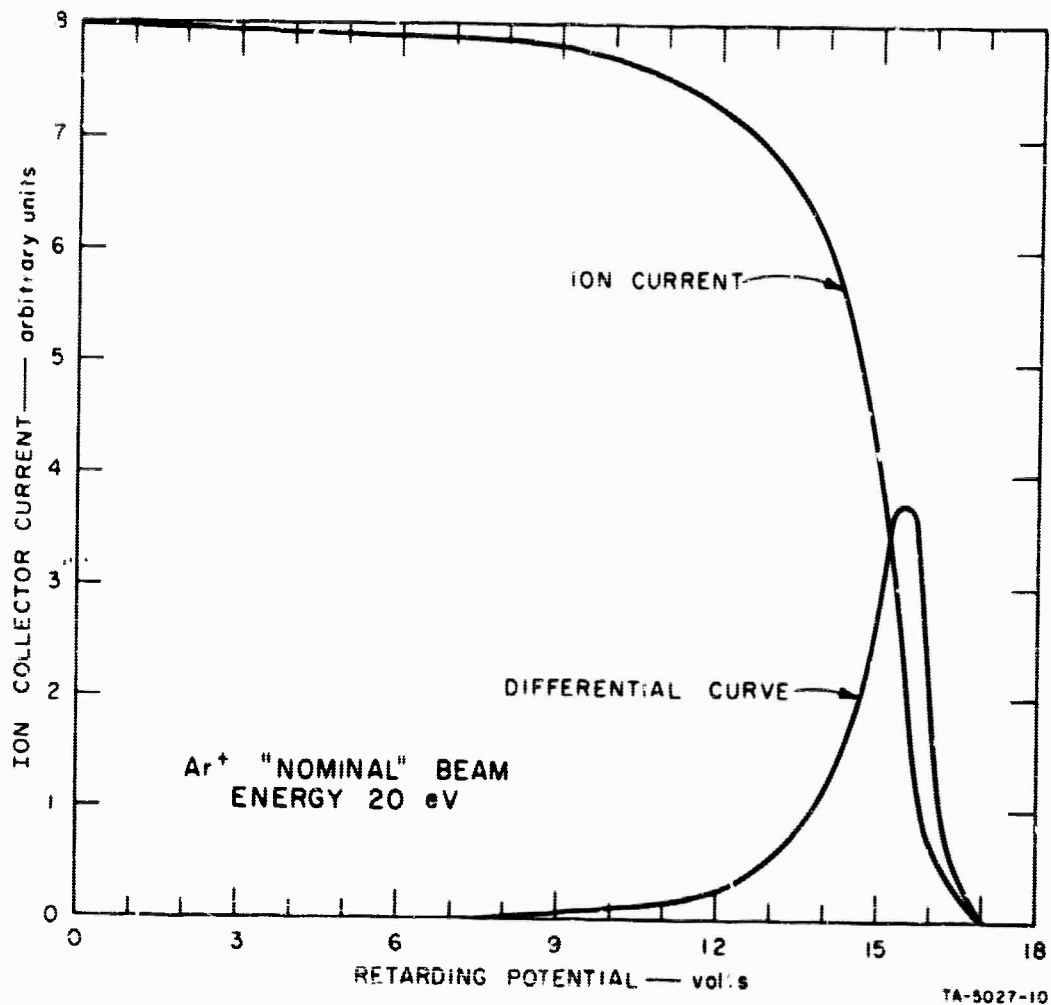
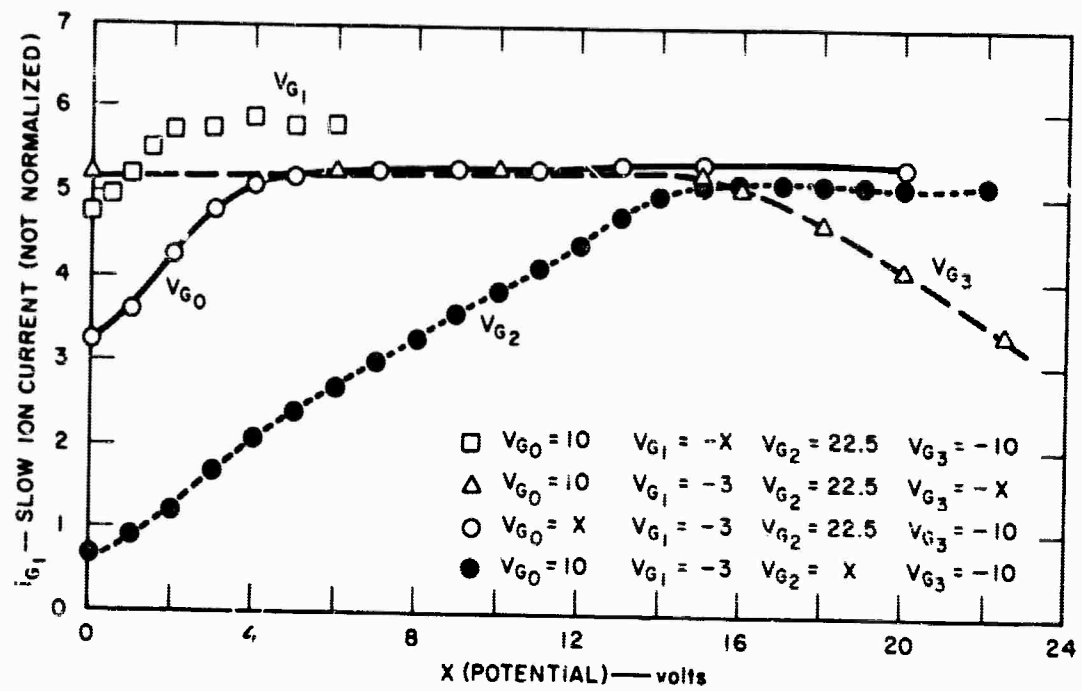


FIG. 2 RETARDING POTENTIAL CURVE FOR Ar<sup>+</sup>



TA-5027-2

FIG. 3 SLOW ION CURRENT SATURATION CURVES

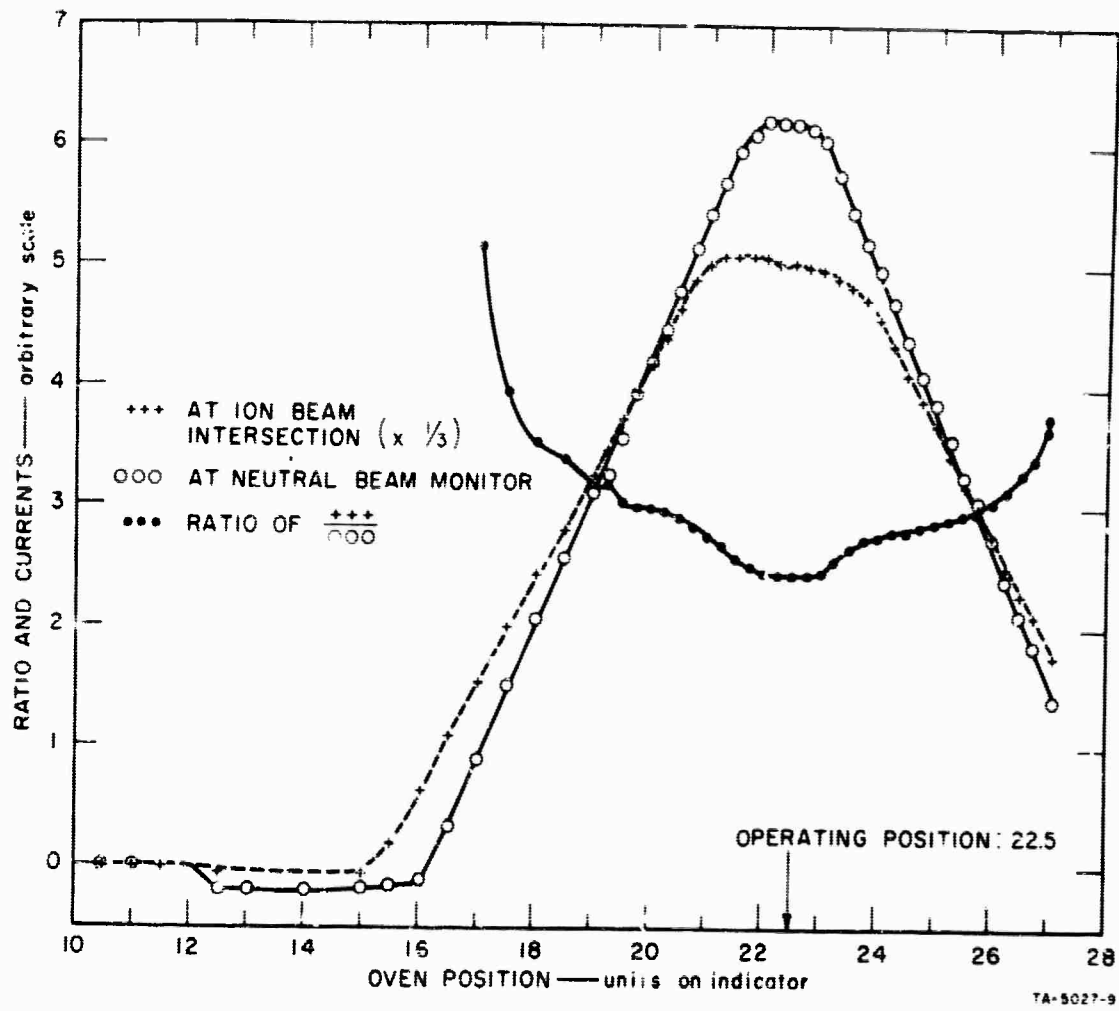


FIG. 4 VAPOR BEAM DETECTOR RESPONSES vs. OVEN POSITION

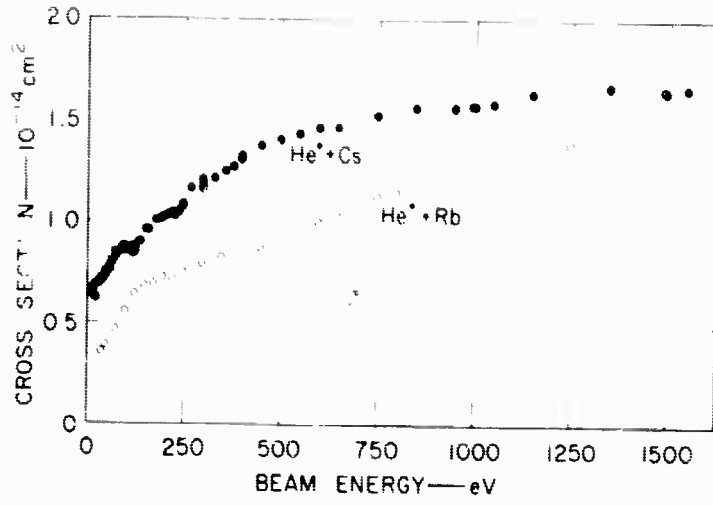


FIG. 5 CROSS SECTIONS FOR  $\text{He}^+$  ON Rb AND Cs vs. ENERGY

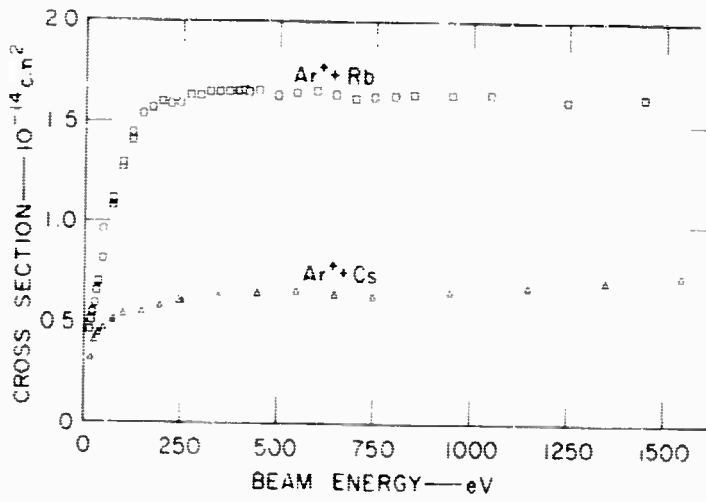


FIG. 6 CROSS SECTIONS FOR  $\text{Ar}^+$  ON Rb AND Cs vs. ENERGY

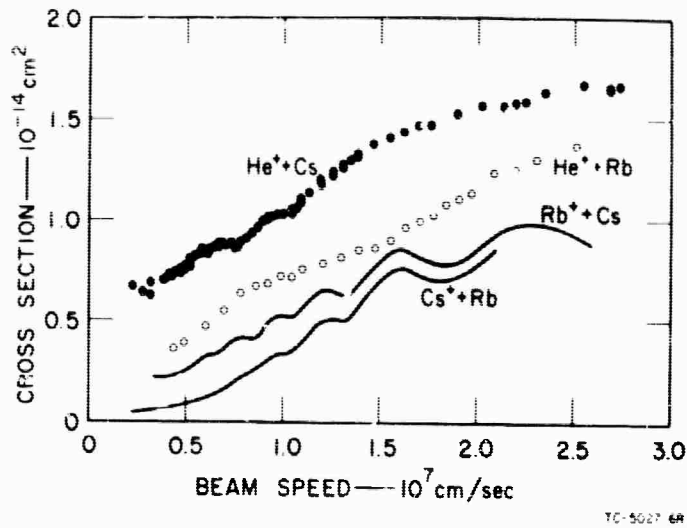


FIG. 7 CROSS SECTIONS FOR  $\text{He}^+$  ON Rb AND Cs vs. VELOCITY

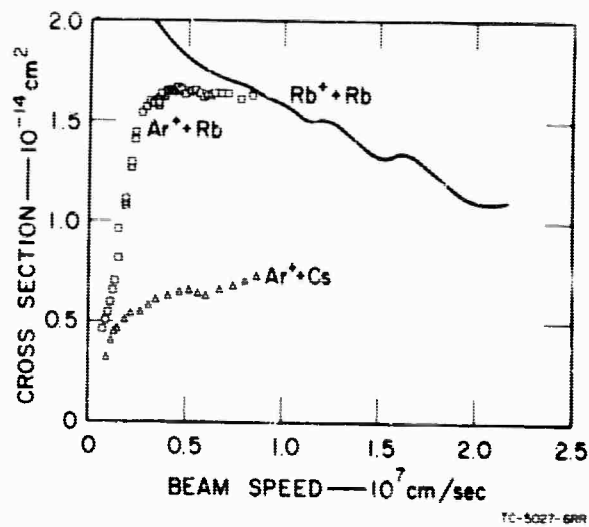


FIG. 8 CROSS SECTIONS FOR  $\text{Ar}^+$  ON Rb AND Cs vs. VELOCITY

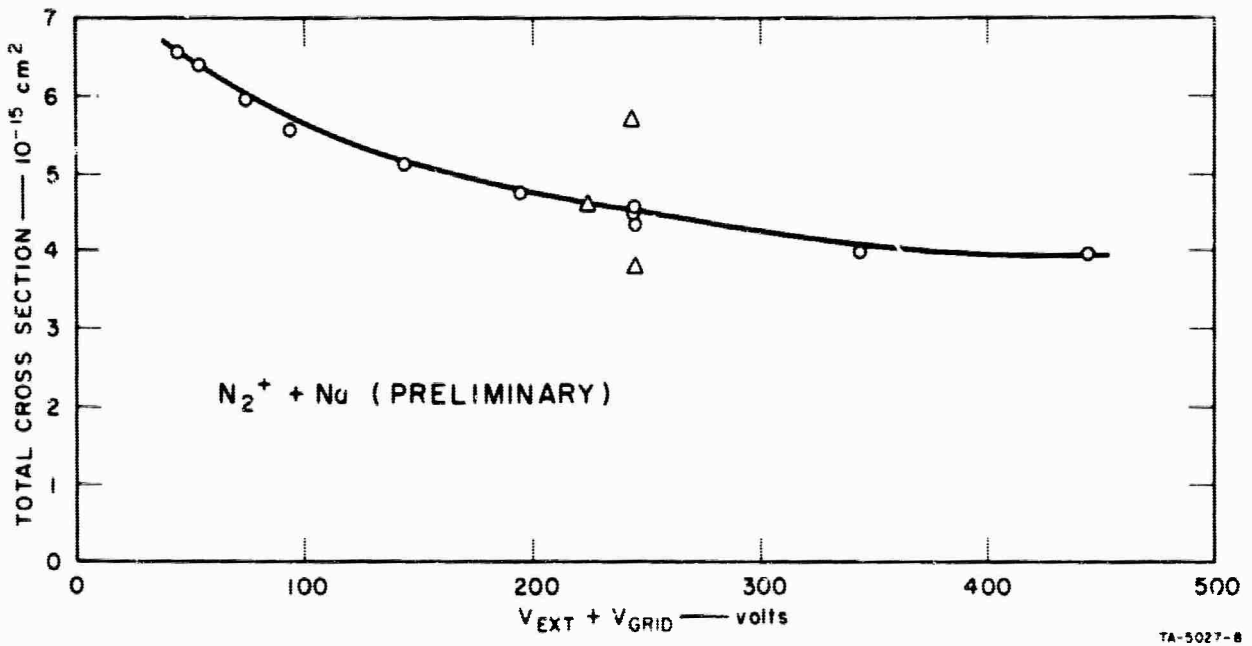


FIG. 9 PRELIMINARY CROSS SECTIONS FOR  $N_2^+$  ON Na vs. ENERGY